Tricuspid Valve Leaflet Strains in Full Heart Preparations via Digital Image Correlation

Trace LaRue[a], Collin E. Haese[b], Alison M. Pouch[c], Jan N. Fuhg[a], Tomasz A. Timek[d], Manuel K. Rausch[a,b,e,f]

[a]*Department of Aerospace Engineering & Engineering Mechanics, The University of Texas at Austin, 2617 Wichita St, Austin, TX, United States of America*
[b]*Department of Mechanical Engineering, The University of Texas at Austin, 204 E Dean Keeton, Austin, TX, United States of America*
[c]*Department of Radiology, University of Pennsylvania, 3700 Hamilton Walk, Philadelphia, PA, United States of America*
[d]*Division of Cardiothoracic Surgery, Corewell Health West, Michigan State University College of Human Medicine, 100 Michigan Ave SE, Grand Rapids, MI, United States of America*
[e]*Department of Biomedical Engineering, The University of Texas at Austin, 107 W Dean Keeton St, Austin, TX, United States of America*
[f]*Oden Institute for Computational Engineering and Sciences, The University of Texas at Austin, 201 E 24th St, Austin, TX, United States of America*

Abstract

Tens of millions across the world have tricuspid valve disease. Understanding the mechanics of the valve is important to diagnosing and treating those patients. The objective of our current work is to fill remaining gaps in our knowledge about tricuspid valve mechanics. Specifically, we are interested in quantifying the between-leaflet and within-leaflet strain heterogeneity under varying hemodynamic and mechanical boundary conditions. To this end, we mounted whole porcine hearts in-vitro, speckled their leaflets, and measured leaflet strains using 3D digital image correlation. We did so while varying peak pressure (20-80 mmHg) and annular dilation (0-60%). To analyze our multi-level data we used linear mixed models. We found that leaflet strains show high within- and between-leaflet heterogeneity, with both depending on pressure but not on annular dilation. Additionally, we found strains to be directionally dependent. The ratio between radial and circumferential strains, i.e., their anisotropy, also depended on pressure. Finally, we found no apparent pattern of strain distributions across the anterior or posterior leaflet. That is, strains near the annulus, in the belly, and near the free edge did not differ significantly. In contrast, we found that strains in the septal leaflet decreased between the annulus and the free edge. Given the complexity of our data, we make all our raw data openly available for others to access and analyze. In conclusion, our data provides a detailed account of the strains in the tricuspid valve leaflets and may form a foundation for future leaflet-specific diagnostic and therapeutic approaches.

Keywords: Anisotropy, Heterogeneity, Annular Dilation, Pressure, Radial, Circumferential, Maximum Principal, In-Vitro Flow Loop, Cardiovascular Mechanics

1. Introduction

Tricuspid valve disease affects millions of Americans, with over 80% of the population developing some degree of valvular leakage during their lifetime [1]. Fortunately, regurgitation remains mild for most. However, in approximately 1.6 Million Americans and many more across the world, tricuspid regurgitation becomes severe enough to affect their quality of life and life expectancy [2]. Historically, tricuspid valve disease was under-treated even in those in whom the disease was severe [3, 4]. Recent advances in surgical and interventional therapy, however, have led to more aggressive treatment [5]. Valve replacement and repair are among two of the available therapeutic options, while the latter is generally preferred as it preserves the native valve and has higher longevity [6, 7, 8]. Such repairs can be performed surgically during open heart surgery or interventionally, i.e., using minimally invasive technology [5, 9]. Either strategy requires knowledge of the valve and should account for the heterogeneous valve anatomy, physiology, and mechanics. For example, surgical incisions and subsequent sutures should be placed in regions of low strain to avoid pull-out [10, 11]. Similarly, clipping devices used in transcatheter edge-to-edge repair should consider local mechanics to prevent device failure [12, 13, 14, 15]. However, this can be challenging given the limited locally resolved data available for the tricuspid valve.

Prior efforts have explored the heterogeneous mechanics of the tricuspid valve. First, Spinner et al. used photogrammetry to quantify leaflets strains in excised porcine valves [16]. However, their analysis was limited to global strains without providing spatially resolved data for each leaflet. Next, Amini Khoiy et al. implanted sonomicrometry crystals in full porcine heart preparations but limited their analysis to the septal leaflet alone [17]. Also using sonomicrometry, but in-vivo, Mathur et al. quantified tricuspid valve leaflet strains in sheep across all three leaflets [18]. Again, the limited spatial resolution of sonomicrometry restricted the level of detail in their findings.

Finally, computational studies have also investigated the mechanics of the tricuspid valve. These studies provide both high-fidelity spatial information and include all valve leaflets. As several examples, we highlight the work by Singh-Gryzbon et al., who built a detailed model of the tricuspid valve from micro-CT imaging; Johnson et al., who used a novel computational framework; and our own work, in which we built subject-specific models of human valves [19, 20, 21, 22]. However, none of these computational studies have been validated sufficiently against ground-truth experimental strain data to guarantee the accuracy of their highly resolved information.

The aim of our current work is to address this knowledge gap by providing spatially resolved information on the mechanics within and between all three tricuspid valve leaflets. Specifically, we will calculate strain as a measure of leaflet mechanics in whole heart preparations using 3D digital image correlation (DIC). Moreover, we will report strains as a function of pressure and annular dilation, and evaluate its orientation dependence to characterize the leaflets' mechanical anisotropy.

2. Methods

2.1. Whole Heart Preparation

In this study, we used whole porcine hearts purchased from a local abattoir. Upon receipt, all hearts were frozen and stored at -80 °C until tested. Before testing, we removed the right atria of the hearts and speckled the tricuspid valve leaflets using an airbrush (Product, Brand) and ink from a pigment liner (GEOTEC School and Office Supplies GmbH, Wörgl, Austria).

2.2. Annular Shape Templates

One challenge of using postmortem whole heart preparations is the lack of information about the in-vivo valve configuration. That is, we do not know the in-situ shape of the annulus or the position of the papillary muscles. While an inherent limitation to our approach, we tried to minimize the uncertainty introduced through this limitation by ensuring a common tricuspid valve annular configuration across all valves. To this end, we created a 3D-printed annular template with a long-axis to short-axis ratio of X and a cross-sectional area of 650 mm^2, which we found fit all our hearts well. Additionally, we created scaled replicas of this template with 30% and 60% of the original's effective orifice area. We subsequently refer to these as the 0%, 30%, and 60% dilation templates.

2.3. Valve Mounting

Next, we used a suture template to mark mounting points around the tricuspid valve annulus. The suture points were next sewn to an adjustable annulus mount. The mount itself featured mount arms with which we adjusted the annular shape to match the 0%, 30%, or 60% dilation template (depending on the experiment). After, we inserted an 5/8" Acetol tube into the pulmonary artery trunk of the hearts and sealed them using cable ties. Finally, we attached the heart to a custom 3D-printed mount. In turn, we attached the mounted heart to the bottom of an acrylic container (9" x 9" x 9") and filled the container with water.

2.4. Experimental Setup & Protocol

The experimental setup is shown in Figure 1. It consisted of the acrylic container with the prepared and mounted heart and a visual access assembly that ensured an even visual field for image acquisition. Additionally, the setup included two high-resolution digital cameras (Imager CX-5, LaVision GmbH, Göttingen, Germany), an illumination source (LED Illumination Unit, LaVision GmbH, Göttingen, Germany), and three water-filled containers that were arranged at 11", 27", and 43" to produce static water columns of 20 mmHg, 50 mmHg, and 80 mmHg, respectively. Finally, the tubing attached to the pulmonary artery was connected through check valves to one of the three elevated water containers and a pressure transducer (5 psig PX409, Omega Engineering Inc., Norwalk, CT).

During experimentation, we first adjusted the annular mount to the 0% configuration and connected the pulmonary artery tubing to the 20 mmHg pressure source while recording images of the atrial surface of the valve with both DIC cameras at 33 Hz. Simultaneously, we recorded pressure in the tubing using the pressure transducer. The target pressure was reached within four seconds, at which point the valve had closed and the experiment concluded. We repeated this experiment by applying 50 mmHg and then 80 mmHg. before adjusting the annulus to the 30% and 60% configuration and repeating above experiments.

2.5. Digital Image Correlation

We conducted DIC using DaVis 11 (LaVision GmbH, Göttingen, Germany). To this end, we loaded the atrial images of each valve (2448 x 2064 pixels) from both cameras and pre-processed them within DaVis. To enhance speckle contrast, we normalized the images by pixel intensity. After processing, we conducted image correlation in two phases. In Stage 1, we chose the 5 mmHg state – when the leaflets first coapt – as our reference configuration and correlated images up to 15 mmHg. In Stage 2, we chose the image at 15mmHg as our reference and correlated images up to the peak pressure of 20, 50, or 80 mmHg, depending on the experiment. We split our analysis into two phases to maximize the visible and, thus, correlatable leaflet surface. That is, in the image at first coaptation the leaflet surfaces are only partially visible. Given the nature of DIC, this partial view would limit correlation, and thus strain information, to only those areas currently visible. All areas that are only visible under higher pressures would remain un-analyzed. See Figure 2 for

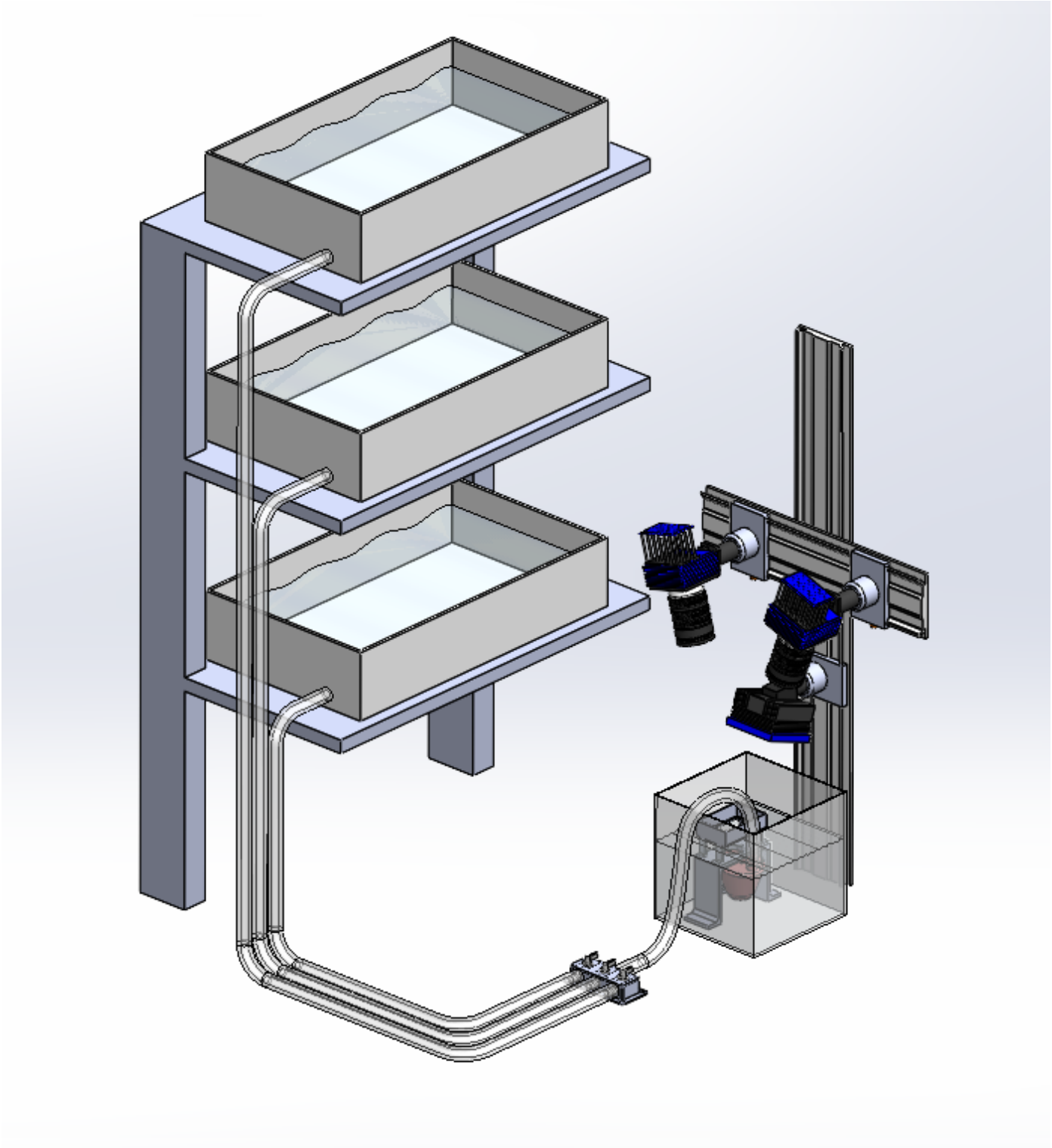

Figure 1: In-vitro whole heart preparation. We mounted whole hearts in a fluid chamber, removed their atria, speckled their leaflets, and finally recorded leaflets strains via 3D Digital Image Correlation (DIC). During testing, we varied pressure by connecting the heart preparations to water columns equivalent to 20, 50, and 80 mmHg. Additionally, we varied annular dilation using a 3D-printed custom annular mount.

a sample data set with raw images, processed images, and correlated images in Stages 1 and 2. For the DIC analysis itself, we chose a subset size of 31 pixels with a step size of 11 pixels. Finally, we exported all correlation data as Green-Lagrange strain in a software-chosen global Cartesian coordinate system.

2.6. Data Analysis

After exporting the data, we post-processed them in Matlab (Version R2024b, Mathworks, Natick, MA). Here, we first projected the strains onto the leaflet surfaces and defined leaflet-specific local coordinate systems. Specifically, we manually chose coordinates for the valve center and defined a radial axis between each leaflet point and the valve center. We defined the circumferential axis as the axis orthogonal to both the local radial direction and the local leaflet surface normal. Finally, we transformed the global Green-Lagrange strain tensor into each local coordinate system. Subsequently, we report maximum principal, radial, and circumferential Green-Lagrange strain. Per leaflet, we obtained approximately 1,000 spatial points and corresponding strains. We additionally removed any duplicate or outlier points. To report within-leaflet strain distributions, we divided the points according to their relative positions between annulus and free edge into near annulus, belly, and free edge [23, 24, 25].

2.7. Statistical Analysis

We report all strain values as means $\pm$ one standard deviation. To test and report the dependence of strains on annular dilation, strain type or strain orientation, pressure, relative position, and leaflet, as well as their interactions, we use a linear mixed model. Specifically, we used the afex library in R (Version 4.1.2, The R Foundation, Vienna, Austria). All multicomparisons were conducted using the "emmeans" library, also in R. We defined statistical significance as p ¡ 0.05.

3. Results

We analyzed leaflet strains in two stages. During Stage 1, we quantified strains between a pressure of 5 and 15 mmHg, and in Stage 2 we quantified strains between 15 mmHg and the target peak pressure (20, 50, or 80 mmHg). Figure 3 summarizes our findings in which we grouped strains across all degrees of dilation and target pressures (for Stage 2). Figure 3A shows mean maximum principle, radial, and circumferential strains across the anterior, posterior, and septal leaflets for Stage 1, i.e., at small pressures. We found that the strains are statistically different between leaflets (p¡0.001) and are statistically different between the radial and circumferential directions (p¡0.001). We also found significant interactions between leaflets and local directions (p¡0.001). However, we found no difference with degree of dilation (p=0.7757). In detail, we found that mean strains differ between leaflets depending on strain type. For maximum principal strain, the posterior leaflet had larger mean strain than the anterior (p¡0.001) and the septal leaflets (p=0.0322), while the septal and anterior leaflet mean strains did not differ (p=0.1046). For the radial strain, the posterior leaflet, again, had larger strains than the anterior (p¡0.001) and the septal (p¡0.001) leaflets, while the anterior leaflet had larger mean strains than the septal leaflet (p=0.0022). Finally, for circumferential strain both the posterior (p=0.0207) and the septal (p=0.0078) leaflets had larger mean strains than the anterior leaflet. There was no difference for circumferential strain between the posterior and septal leaflets (p=0.9429). When inspecting the difference between mean radial and circumferential strains, we found that radial strain is larger than the circumferential strain in the posterior leaflet (p¡0.001). In contrast, the radial strain is smaller than the circumferential strain in the septal leaflet (p¡0.001). In the anterior leaflet, there was no statistical difference between the mean of both strains (p=0.4401). In summary, at small pressures mean leaflet strains differ between leaflets and directions.

Figure 3B shows the mean maximum principle, radial, and circumferential strains across the anterior, posterior, and septal leaflets for Stage 2, i.e., large pressures. As expected at higher pressures, we found that strains in Stage 2 are larger than in Stage 1. Please note that the strain analysis in Stage 2 includes one additional variable, peak pressure (20, 50, 80 mmHg) in addition to leaflet and strain direction. However, in the figure we grouped strains for all pressures. For the complete data, please see our data availability statement for raw data tables. Quantitatively, we found that strain, again, depends on leaflet (p¡0.001) and direction (p¡0.001), and also pressure (p¡0.001). At high pressures, too, we found that strains do not depend on the degree of dilation (p=0.5526). Additionally, we found significant interactions between pressure and leaflet (p¡0.001), pressure and direction (p¡0.001), and leaflet and direction (p¡0.001). For simplicity, we limit our results to a general description of these findings, but refer the interested reader to 6 with a detailed list of all comparisons between pressures, leaflets, and directions. Overall, we consistently found that all strains in all leaflets increase with pressure. Furthermore, we found that the relative magnitude between radial and circumferential strains is mostly invariant to peak pressure. Specifically, we found that mean circumferential strain was generally larger than radial strain in the anterior and the septal leaflets, while the opposite was true for the posterior leaflet. For the posterior and septal leaflet, these findings are consistent with the direction-dependence we found in Stage 1. Finally, we found that the relative strain between leaflets is mostly invariant to pressure. That is, maximum principal and circumferential strain are consistently largest in the septal leaflet than the anterior leaflet, and smallest in the posterior leaflet. For radial strains, the relative magnitude depends on the pressure levels and a detailed account is providing in the 6. In summary, mean strains increase with pressure across all leaflets while their anisotropic distribution and their heterogeneity among leaflets is mostly invariant to pressure.

We also multiplicatively combined strains of Stage 1 and 2 and, thus, computed total leaflet strains. Our sta-

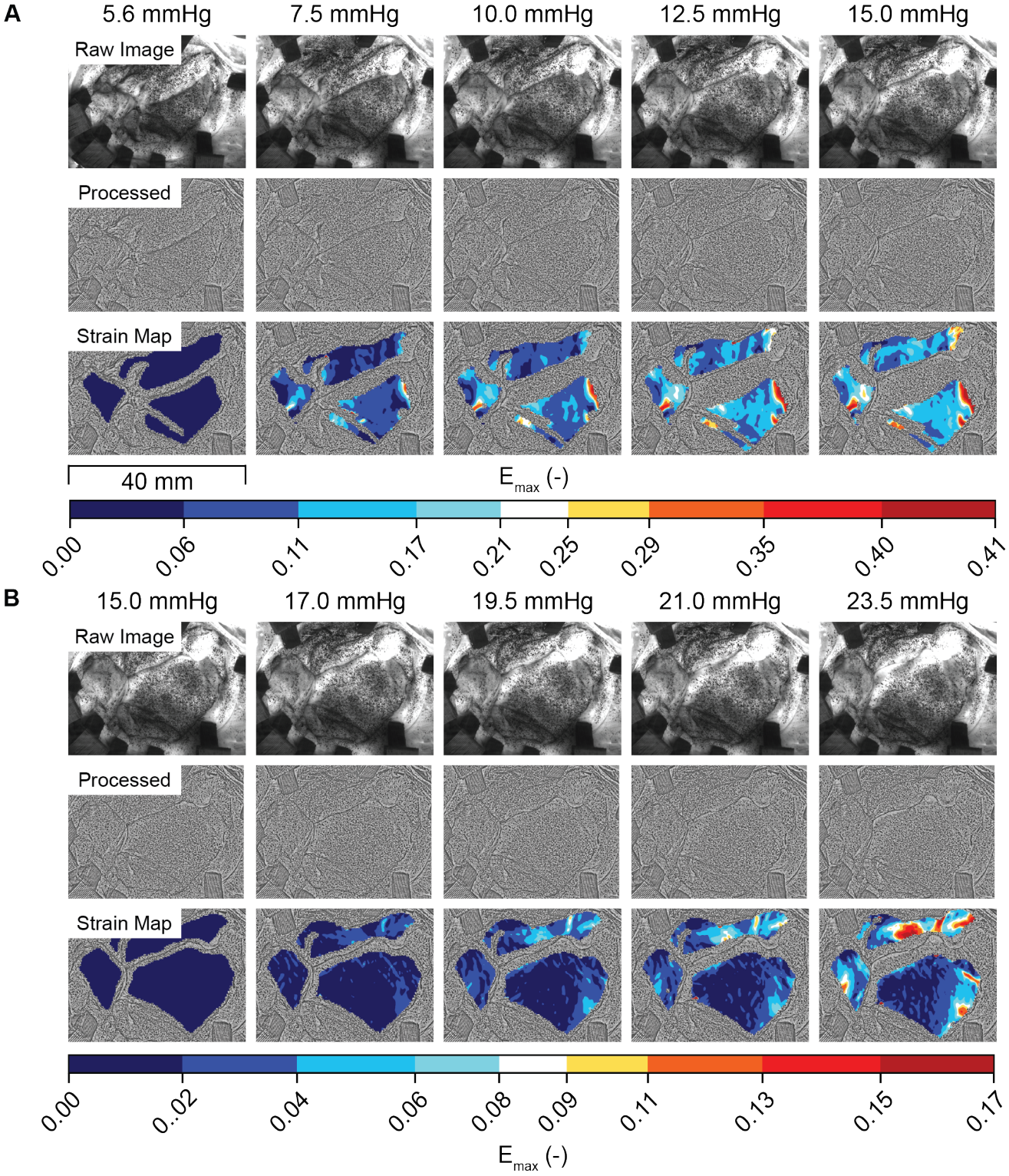

Figure 2: Sample data from 3D Digital Image Correlation. We first recorded speckled leaflet images with two digital cameras before processing the data for contrast normalization. Finally, we used DaViz 11 to correlate images and derive surface strain maps across each leaflet. Please note, we did so in two stages: A) In Stage 1 we tracked images between 5 and 15 mmHg; B) In Stage 2 we tracked images between 15 mmHg and target pressures 20, 50, or 80 mmHg.

tistical findings closely reflect those of the two-stage analysis. That is, total strains depend on leaflet, direction, and pressure (all p¡0.001), but not dilation (p=0.957). Additionally, all interactions between leaflet, direction, and pressure are significant (all p¡0.001). A detailed list of all comparisons between pressures, leaflets, and directions

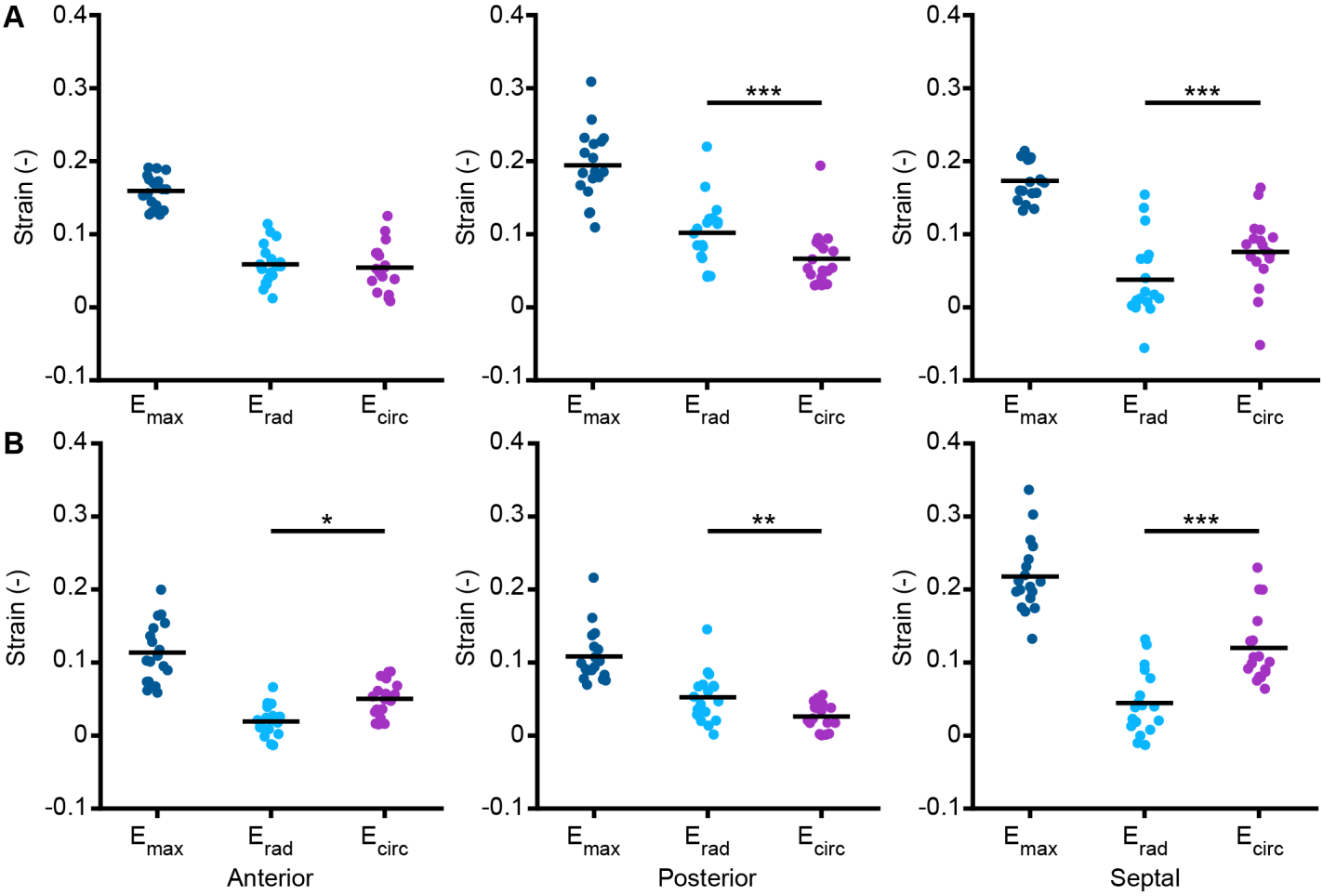

Figure 3: Between-leaflet heterogeneity and anisotropy of tricuspid valve strains. A) Strains induced between 5 mmHg and 15 mmHg (Stage 1). B) Strains induced between 15 mmHg and 20-80 mmHg. Please note, we grouped strains across all degrees of dilation and target pressures (for Stage 2). E_{max} = maximum principal Green Lagrange strain; E_{rad} = radial Green Lagrange strain; E_{circ} = circumferential Green Lagrange strain.

is again available in the 6 and all tabulated raw data are available. In short, we found that strains increase with pressure. Furthermore, we found that the relative magnitude between radial and circumferential strains is mostly invariant to peak pressure. As in Stage 2, here, we found that mean circumferential strain was generally larger than mean radial strain in the anterior and the septal leaflets, while the opposite was true for the posterior leaflet. Finally, we found that the relative strain between leaflets is mostly invariant to pressure. Specifically, we found that maximum principal and circumferential strain are consistently larger in the posterior than the anterior leaflet. This contrasts our findings of Stage 2 in which this relationship was reversed. Consistent with Stage 2, we found that maximum principal and circumferential strains are larger in the septal than the anterior and the posterior leaflet. Finally, for radial strains, as in Stage 2, we found that the relative strain magnitude depends on the peak pressure. In summary, combining strains from Stage 1 and Stage 2 suggests that strains increase with pressure across all leaflets while their anisotropic distribution and their heterogeneity among leaflets is mostly invariant to pressure.

Figure 4 shows the combined maximum principal, radial, and circumferential strains as a function of pressure for each leaflet. For illustrative purposes, we fit an exponential function to these data. We interpret the slopes of these curves as “effective compliance” as they are not material inherent, but depend on both structural parameters – such as leaflet thickness – and boundary conditions – such as chordal insertions. Nonetheless, these data suggest the effective compliance differs with direction, i.e., is generally higher in the radial direction than the circumferential direction. Moreover, these data suggest that the anterior leaflet is less compliant in the radial direction than the septal and posterior leaflets. Additionally, these data suggest that the septal leaflet is the most compliant of the three in the circumferential direction.

Until now, we have reported all strains as mean values across the anterior, posterior, and septal leaflets. Figure 5 shows strains across the whole leaflets as functions of pressure and leaflets for Stage 1, Figure 5A, and Stage 2, Figure 5B-D. Clearly, strains are widely distributed across

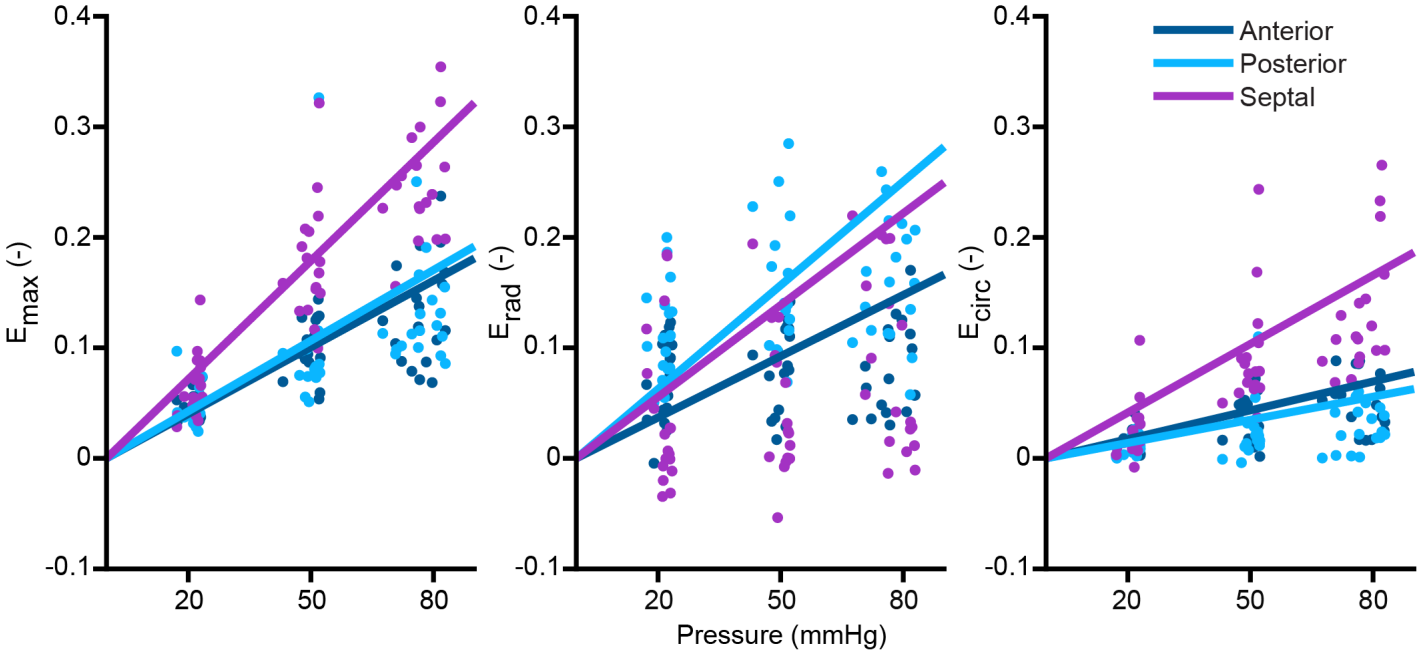

Figure 4: Strain as a function of pressure for each leaflet. Fitted lines are least square regressions of an exponential function. E_{max} = maximum principal Green Lagrange strain; E_{rad} = radial Green Lagrange strain; E_{circ} = circumferential Green Lagrange strain.

each leaflet with strains of 0.161 $\pm$ 0.093, 0.197 $\pm$ 0.088, and 0.177 $\pm$ 0.098 for the anterior, posterior, and septal leaflets in Stage 1, respectively. Interestingly, for a target pressure of 20 mmHg, the strain distributions significantly narrow as indicted in 5B. That is, we found strains of 0.044 $\pm$ 0.037, 0.041 $\pm$ 0.024, and 0.055 $\pm$ 0.039 for the anterior, posterior, and septal leaflets. With increasing pressure, i.e., 50 and 80 mmHg target pressure, the distribution means increase and widen relative to 20 mmHg (50mmHg: 0.086 $\pm$ 0.064, 0.083 $\pm$ 0.041, and 0.150 $\pm$ 0.094; 80mmHg: 0.114 $\pm$ 0.098, 0.108 $\pm$ 0.057, and 0.218 $\pm$ 0.132, for the anterior, posterior, and septal leaflets, respectively) as shown in 5C-D. Among the three leaflets, the septal leaflets stands out as showing the widest strain distribution, i.e., the most heterogeneity.

Finally, we divided strains across the leaflets into three categories according to their relative position between the annulus and the free edge: “Free Edge”, “Belly Region”, “Near Annulus.” We did so only for Stage 2 because the belly and free edge regions are, at least partially, hidden at small strains and can thus not be included in our strain analysis. Figure 6 illustrates strains for all leaflets divided by regions. Please note that we grouped results for all degrees of dilation and all target pressures. Statistically, we find that strains depend on region only in the septal leaflets, but not the anterior or posterior leaflets. Within the septal leaflet maximum principal strain differs between the near annulus and free edge ($p<0.001$) and the belly and the free edge ($p=0.008$). Radial strain differs between the near annulus and the belly as well as the near annulus and the free edge (both $p<0.001$). Finally, circumferential strain differs between annulus and belly ($p=0.0234$) as well as free edge ($p<0.001$), and between belly and free edge ($p=0.008$). In summary, within-leaflet heterogeneity is limited to the septal leaflet in which strains differ between the near annulus, belly, and free edge regions.

4. Discussion

Tricuspid valve mechanics are a critical determinant of its function and dysfunction. Understanding the valve’s response to hemodynamic and mechanical loading may provide a mechanistic insight into why the valve fails in millions of patients and suggest how to best repair it [26, 27]. To date, there are few studies that have investigated the valve’s mechanical response and none of these have compared the mechanics of the three leaflets as well as the mechanical heterogeneity within each leaflet. In our current work, we combined an in-vitro heart flow loop with 3D DIC to spatially resolve strains across each leaflet and within each leaflet. We did so under physiological and pathological pressures as well as under varying degrees of annular dilation.

Unsurprisingly, we found that the mechanics of the tricuspid valve are complex. Most importantly, we found that there is high heterogeneity in strains among the leaflets and within the leaflets. We also found that leaflet strains are anisotropic and that this anisotropy differs between the leaflets. Interestingly, we found that dilation – even when very large – had no effect on leaflet strains.

To our negative finding first: We found that dilating the annulus to 30% and 60% of our original effective orifice

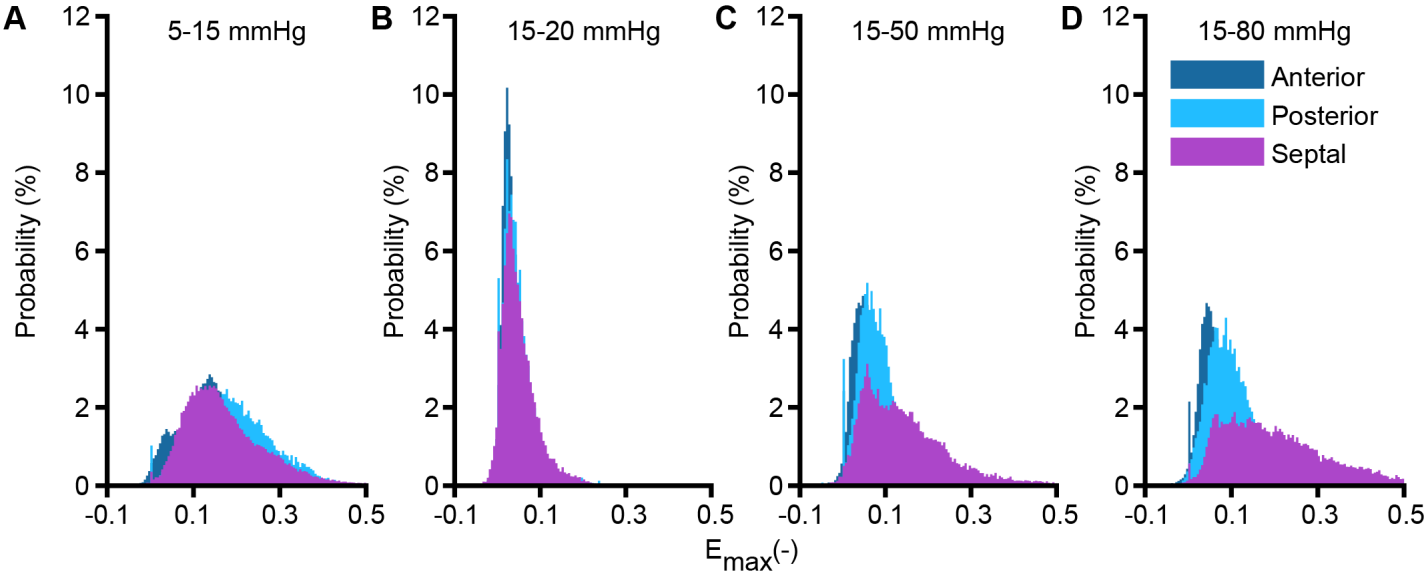

Figure 5: Maximum principal strain distributions across each leaflet. A) Strains induced between 5mmHg and 15 mmHg (Stage 1). B) Strains induced between 15 mmHg and 20-80 mmHg. Please note, we grouped strains across all three degrees of dilation.

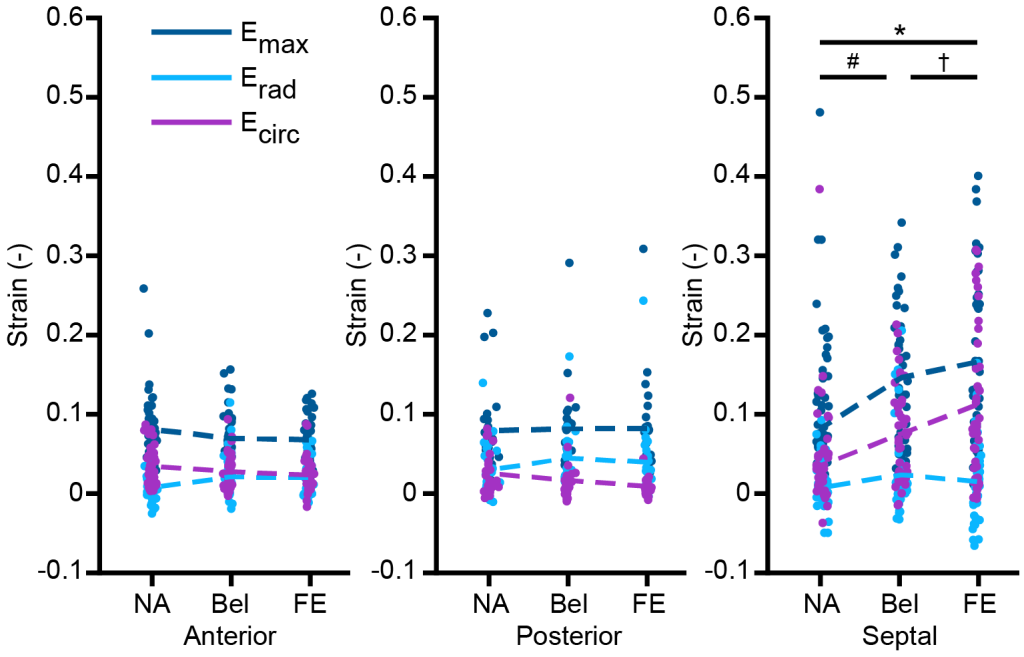

Figure 6: Spatial distribution of strains within all three leaflets. Please note, we grouped strains across all three pressure levels and degrees of dilation. E_{max} = maximum principal Green Lagrange strain; E_{rad} = radial Green Lagrange strain; E_{circ} = circumferential Green Lagrange strain.

area did not change leaflet strains. This finding is unexpected and contradicts ours and others' prior assumptions. Importantly it should be noted that even at 60% dilation, no leakage was observed. Us and others have previously assumed that leaflet strain – and therefore stress – would increase with increasing dilation [26, 28, 29]. Often, Laplace's law is cited which suggests that increasing diameter leads to increasing tension [30, 31, 32]. This remains a crude assumption given the many ways in which the tricuspid valve fails to meet the assumptions of a thin-walled sphere. We suspect that the complexity of the leaflet geometry, the importance of the leaflet contact mechanics, and the insertion of chordae tendineae within the leaflets together render Laplace's equation a poor approximation for the complex mechanics of the tricuspid valve. We also suspect that our finding may change once the annulus dilates enough to induce regurgitation. That is, we expect that hemodynamic changes and insufficient con-

tact may alter leaflet strains, especially close to the leaflet free edge [23, 26, 33]. However, future studies will have to test this hypothesis. For now, our findings provide critical insight into the lack of sensitivity of valve mechanics to "moderate" annular dilation.

To our positive findings: we found that strains differ across the three leaflets and we showed this between-leaflet heterogeneity through multiple comparisons. First, we found that strains magnitudes differ between leaflets with strains generally being larger in the septal leaflet than in the anterior and posterior leaflets, while we found that strains between the anterior and posterior leaflets are generally comparable. Please note that the specific findings are highly nuanced as the exact relationship between leaflets depended, for example, on pressure. Similarly, we found that strains differ with direction. However, no clear pattern emerged. In the posterior leaflet radial strains exceeded circumferential strains, while this relationship was reversed in the anterior and septal leaflets. Here, again, these general patterns were complicated by dependencies on pressure. In short, while some general patterns emerge, between-leaflet heterogeneity and anisotropy are complex.

Additionally, our full-field DIC technique enabled spatial quantification of strain across the majority of the leaflet surfaces. We found that strains were highly heterogeneous across the leaflets. This heterogeneity likely stems from leaflets thickness heterogeneity which we have reported previously, as well as chordal insertion sites that impact leaflet strains [23, 28]. Interestingly, no simple spatial pattern emerged. That is, we tested whether strains near the annulus, the leaflet belly, or the near edge differed, but found signficant results only in the septal leaflet. Additionally we found that the "degree of heterogeneity" as measured by the strain distribution width differed among leaflets and with pressure. It appeared that increasing pressure widened the strain distributions in all leaflets and that the septal leaflet had notably larger strain heterogeneity. This latter finding is consistent with previous reports that point out the uniqueness of the septal leaflet [34, 18, 24, 28]. For example, we have previously shown that chordal insertions into the septal leaflet differ significantly from those of the anterior and posterior leaflet [24, 25].

Although our work is unique for its report of full strain fields, our findings are – at least in part – comparable to prior work by others and ourselves. For example, Spinner et al. have previously reported leaflet strains across two porcine leaflets (anterior and posterior), while ignoring the septal leaflet and not reporting on spatial heterogeneity [16]. Overall, their reported stretches are of similar magnitude to our reported strains. For example, they reported "maximum axis stretch ratios" of 1.17 and 1.54 for their anterior and posterior leaflets, respectively. These stretch translate to strains of 0.18 and 0.69 at 50 mmHg. Consistent with our findings, annular dilation in their study did not induce any statistically significant differences in leaflet strains. Additionally, they found strains to be larger in the posterior leaflet than the anterior leaflets, which agrees with our finding for that same pressure and same strain measure (maximum principal strain). In another study, Amini Khoiy et al. used whole porcine hearts in-vitro to measure septal leaflet strains using sonomicrometry crystals [17]. Interestingly, their reported strains were significantly smaller than ours. That is, they reported maximum principal strains of 0.112 at a pressure of 30 mmHg. They also found no anisotropy and did not test for heterogeneity. Thus, only limited comparison between our findings are possible. Finally, in comparison to our own work, Mathur et al. reported in-vivo ovine strains similar to those of our current study [18]. For example, we previously found in-vivo maximum principal strains of 0.47, 0.31, and 0.65 (when averaged across "regions") for the posterior, septal, and anterior ovine leaflets, respectively. We note that our ability to investigate spatial heterogeneity in our prior in-vivo study was severely hampered by the poor spatial resolution of the sonomicrometry based technique which only allowed for calculating strains at two locations in the leaflet. In contrast to our current study, we previously found that radial strains were larger than circumferential strains and that the anterior leaflet had the largest strains. Overall, our findings are in good agreement with prior studies where comparison is possible. Disagreements likely stem from using different strain measurement techniques, different experimental settings (in-situ versus in-vitro versus in-vivo) and inter-species differences.

Of course our study is subject to limitations. Most importantly, our study was conducted in explanted porcine hearts which has important implications. First, our hearts do not contract. Thus, we ignore the complex hemodynamics of a beating heart and the dynamism of the tricuspid annulus and the papillary muscles. Additionally, the impact of post-mortem changes to tissue properties may impact material stiffness and thus our strain measurements. Also, we did not know the native in-vivo shape of the tricuspid annulus or the position of the papillary muscles. We assumed a common in-vivo annular configuration for all valves. As to the papillary muscles, we accepted their natural position within the myocardium. Both limitations likely affect our findings. In future studies, we plan on using in-vivo imaging to extract both annular shape and papillary muscle positions to build subject-specific annular and papillary muscle mounts. Lastly, we studied the tricuspid valve mechanics at static pressures which ignores any inertial effects on leaflet mechanics.

5. Conclusion

In our work we provide a comprehensive in-vitro analysis of tricuspid valve leaflet strains. Our analysis investigates between-leaflet heterogeneity, within-leaflet heterogeneity, mechanical anisotropy, and the role of annular dilation and pressure. Overall, we found that leaflet strains

are highly heterogeneous between and within leaflets. We further found that strains increase with pressure and, surprisingly, are independent of annular dilation. We also found that strains in the near annulus region, in the belly region, and the near free edge only differ in the septal leaflet, but not the anterior or posterior. Through these findings, our work fills an important knowledge gap about the mechanics of the tricuspid valve.

6. Appendix

Dilation (%)	**Anterior**	**Posterior**	**Septal**
	Phase 1: 5-15 mmHg		
0	0.166±0.097	0.195±0.094	0.176±0.110
30	0.164±0.096	0.208±0.087	0.172±0.084
60	0.154±0.087	0.186±0.082	0.183±0.100
	Phase 2: 15-20 mmHg		
0	0.045±0.034	0.031±0.019	0.067±0.046
30	0.041±0.029	0.037±0.021	0.054±0.040
60	0.048±0.048	0.053±0.031	0.043±0.029
	Phase 2: 15-50 mmHg		
0	0.088±0.063	0.067±0.039	0.162±0.100
30	0.087±0.070	0.103±0.047	0.148±0.096
60	0.083±0.059	0.079±0.037	0.140±0.086
	Phase 2: 15-80 mmHg		
0	0.116±0.097	0.112±0.072	0.244±0.142
30	0.112±0.108	0.098±0.050	0.206±0.128
60	0.113±0.089	0.114±0.049	0.204±0.126

Table 1: Mean ±1 standard deviation E_{max} for each leaflet, dilation, and pressure over all six hearts.

References

[1] J. P. Singh, J. C. Evans, D. Levy, M. G. Larson, L. A. Freed, D. L. Fuller, B. Lehman, E. J. Benjamin, Prevalence and clinical determinants of mitral, tricuspid, and aortic regurgitation (the framingham heart study), The American Journal of Cardiology 83 (6) (1999-03-15) 897–902. doi:10.1016/S0002-9149(98)01064-9.

[2] J. Nath, E. Foster, P. A. Heidenreich, Impact of tricuspid regurgitation on long-term survival, Journal of the American College of Cardiology 43 (3) (2004-02) 405–409. doi:10.1016/j.jacc.2003.09.036.

[3] E. A. Prihadi, Tricuspid valve regurgitation: no longer the "forgotten valve", e-Journal of Cardiology Practice 16 (30), issue: 30 Volume: 16 (2018-11).

[4] O. Stuge, J. Liddicoat, Emerging opportunities for cardiac surgeons within structural heart disease, The Journal of Thoracic and Cardiovascular Surgery 132 (6) (2006-12-01) 1258–1261, publisher: Elsevier. doi:10.1016/j.jtcvs.2006.08.049.

[5] R. J. Henning, Tricuspid valve regurgitation: current diagnosis and treatment, Am J Cardiovasc Dis 12 (1) (2022-02-15) 1–18.

[6] T. K. M. Wang, B. P. Griffin, R. Miyasaka, B. Xu, Z. B. Popovic, G. B. Pettersson, A. M. Gillinov, M. Y. Desai, Isolated surgical tricuspid repair versus replacement: meta-analysis of 15 069 patients, Open Heart 7 (1) (2020-03-01) e001227, publisher: Archives of Disease in childhood Section: Valvular heart disease. doi:10.1136/openhrt-2019-001227.

[7] W. Wong, S. Chen, A. Chou, H. Lee, Y. Cheng, F. Tsai, K. Lee, V. C. Wu, C. Wang, S. Chang, P. Chu, Late outcomes of valve repair versus replacement in isolated and concomitant tricuspid valve surgery: A nationwide cohort study, Journal of the American Heart Association 9 (8) (2020-04-21) e015637, publisher: Wiley. doi:10.1161/JAHA.119.015637.

[8] D. Hagemeyer, G. Ong, M. D. Peterson, N. P. Fam, Transcatheter tricuspid valve intervention: to repair or to replace?, Current Opinion in Cardiology 37 (6) (2022-11) 495. doi:10.1097/HCO.0000000000000997.

[9] F. Praz, D. Muraru, F. Kreidel, P. Lurz, R. T. Hahn, V. Delgado, M. Senni, R. S. Von Bardeleben, G. Nickenig, J. Hausleiter, A. Mangieri, J. L. Zamorano, B. D. Prendergast, F. Maisano, Transcatheter treatment for tricuspid valve disease, EuroIntervention 17 (10) (2021-11) 791–808. doi:10.4244/EIJ-D-21-00695.

[10] I. D. Madukauwa-David, E. L. Pierce, F. Sulejmani, J. Pataky, W. Sun, A. P. Yoganathan, Suture dehiscence and collagen content in the human mitral and tricuspid annuli, Biomech Model Mechanobiol 18 (2) (2019-04-01) 291–299. doi:10.1007/s10237-018-1082-z.

[11] D. M. Paul, A. Naran, E. L. Pierce, C. H. Bloodworth, S. F. Bolling, A. P. Yoganathan, Suture dehiscence in the tricuspid annulus: An ex vivo analysis of tissue strength and composition, The Annals of Thoracic Surgery 104 (3) (2017-09-01) 820–826. doi:10.1016/j.athoracsur.2017.02.040.

[12] P. Lurz, C. Besler, T. Schmitz, R. Bekeredjian, G. Nickenig, o. H. M, B. R. S. von, A. Schmeisser, I. Atmowihardjo, L. R. Estevez, E. Lubos, M. Heitkemper, D. Huang, H. Lapp, E. Donal, M. Adamo, P. Golino, B. Melica, V. Rudolph, R. Corti, X. Freixa, D. Arzamendi, F. Praz, F. Castriota, K. Veien, M. Kowalski, B. Rensing, N. Schofer, A. Zirlik, W. Rottbauer, Short-term outcomes of tricuspid edge-to-edge repair in clinical practice, Journal of the American College of Cardiology 82 (4) (2023-07-25) 281–291, publisher: American College of Cardiology Foundation. doi:10.1016/j.jacc.2023.05.008.

[13] D. Maj, K. Jasinska-Gniadzik, T. Kopiec, M. Wieteska, A. Gasecka, A. Rdzanek, A. O. Kraaijeveld, K. Pujdak, M. Grabowski, A. Pietrasik, Complications following transcatheter edge-to-edge mitral valve repair: Personal experience and review of the literature, Cardiol J 30 (5) (2023-10-27) 832–842. doi:10.5603/CJ.a2023.0029.

[14] F. M. Asch, S. H. Little, G. B. Mackensen, P. A. Grayburn, P. Sorajja, M. J. Rinaldi, F. Maisano, S. Kar, Incidence and standardised definitions of mitral valve leaflet adverse events after transcatheter mitral valve repair: the EXPAND study, EuroIntervention 17 (11) (2021-12) e932–e941. doi:10.4244/EIJ-D-21-00012.

[15] G. Flores, D. Mesa, S. Ojeda, J. S. de Lezo, R. Gonzalez-Manzanares, G. Dueñas, M. Pan, Complications of the per-

	Anterior		Posterior		Septal	
Dilation (%)	E_{rad}	E_{circ}	E_{rad}	E_{circ}	E_{rad}	E_{circ}
			Phase 1: 5-15 mmHg			
0	0.051±0.073	0.052±0.064	0.110±0.074	0.072±0.048	0.036±0.103	0.069±0.071
30	0.067±0.078	0.049±0.071	0.097±0.064	0.087±0.063	0.030±0.090	0.077±0.073
60	0.068±0.073	0.058±0.082	0.108±0.070	0.062±0.054	0.042±0.098	0.081±0.077
			Phase 2: 15-20 mmHg			
0	0.006±0.022	0.016±0.027	0.009±0.018	0.009±0.014	0.002±0.039	0.027±0.041
30	0.004±0.021	0.015±0.023	0.015±0.016	0.013±0.015	0.001±0.037	0.025±0.036
60	0.007±0.030	0.013±0.032	0.018±0.027	0.012±0.022	-0.003±0.045	0.012±0.023
			Phase 2: 15-50 mmHg			
0	0.020±0.044	0.030±0.044	0.023±0.035	0.021±0.026	0.015±0.069	0.094±0.099
30	0.014±0.039	0.037±0.051	0.055±0.043	0.031±0.034	0.007±0.080	0.085±0.092
60	0.016±0.048	0.031±0.065	0.037±0.040	0.018±0.027	0.015±0.094	0.069±0.066
			Phase 2: 15-80 mmHg			
0	0.024±0.045	0.046±0.066	0.054±0.056	0.023±0.037	0.055±0.108	0.126±0.104
30	0.018±0.043	0.051±0.076	0.039±0.042	0.028±0.040	0.027±0.099	0.125±0.115
60	0.016±0.058	0.053±0.083	0.064±0.049	0.027±0.037	0.052±0.085	0.108±0.106

Table 2: Mean ±1 standard deviation E_{rad} and E_{circ} for each leaflet, dilation, and pressure over all six hearts.

	Anterior	Posterior	Septal
Comparison		p Value	
		Phase 1: 5-15 mmHg	
E_{max} - E_{rad}	<0.0001	<0.0001	<0.0001
E_{max} - E_{circ}	<0.0001	<0.0001	<0.0001
E_{rad} - E_{circ}	0.4411	0.0001	<0.0001
		Phase 2: 15-80 mmHg	
E_{max} - E_{rad}	<0.0001	<0.0001	<0.0001
E_{max} - E_{circ}	<0.0001	<0.0001	<0.0001
E_{rad} - E_{circ}	0.0035	0.0293	<0.0001

Table 3: Statistical comparisons of strains for each leaflet.

cutaneous mitral valve edge-to-edge repair: Role of transesophageal echocardiography, J Clin Med 11 (16) (2022-08-14) 4747. doi:10.3390/jcm11164747.

[16] E. M. Spinner, D. Buice, C. H. Yap, A. P. Yoganathan, The effects of a three-dimensional, saddle-shaped annulus on anterior and posterior leaflet stretch and regurgitation of the tricuspid valve, Ann Biomed Eng 40 (5) (2012-05) 996–1005. doi:10.1007/s10439-011-0471-6.

[17] K. Amini Khoiy, D. Biswas, T. N. Decker, K. T. Asgarian, F. Loth, R. Amini, Surface strains of porcine tricuspid valve septal leaflets measured in ex vivo beating hearts, Journal of Biomechanical Engineering 138 (111006) (2016-10-21). doi:10.1115/1.4034621.

[18] M. Mathur, T. Jazwiec, W. D. Meador, M. Malinowski, M. Goehler, H. Ferguson, T. A. Timek, M. K. Rausch, Tricuspid valve leaflet strains in the beating ovine heart, Biomech Model Mechanobiol 18 (5) (2019-10) 1351–1361. doi:10.1007/s10237-019-01148-y.

[19] S. Singh-Gryzbon, V. Sadri, M. Toma, E. L. Pierce, Z. A. Wei, A. P. Yoganathan, Development of a computational method for simulating tricuspid valve dynamics, Ann Biomed Eng 47 (6) (2019-06) 1422–1434. doi:10.1007/s10439-019-02243-y.

[20] E. L. Johnson, D. W. Laurence, F. Xu, C. E. Crisp, A. Mir, H. M. Burkhart, C.-H. Lee, M.-C. Hsu, Parameterization, geometric modeling, and isogeometric analysis of tricuspid valves, Computer Methods in Applied Mechanics and Engineering 384 (2021-10) 113960. doi:10.1016/j.cma.2021.113960.

[21] M. Mathur, W. D. Meador, M. Malinowski, T. Jazwiec, T. A. Timek, M. K. Rausch, Texas TriValve 1.0 : a reverse-engineered, open model of the human tricuspid valve, Engineering with Computers 38 (5) (2022-10-01) 3835–3848. doi:10.1007/s00366-022-01659-w.

[22] C. E. Haese, M. Mathur, C.-Y. Lin, M. Malinowski, T. A. Timek, M. K. Rausch, Impact of tricuspid annuloplasty device shape and size on valve mechanics—a computational study, JTCVS Open (2023-11) S2666273623003534doi:10.1016/j.xjon.2023.11.002.

[23] W. D. Meador, M. Mathur, G. P. Sugerman, M. Malinowski, T. Jazwiec, X. Wang, C. M. Lacerda, T. A. Timek, M. K. Rausch, The tricuspid valve also maladapts as shown in sheep with biventricular heart failure, eLife 9 (2020-12-15) e63855, publisher: eLife Sciences Publications, Ltd. doi:10.7554/eLife.63855.

[24] W. D. Meador, M. Mathur, G. P. Sugerman, T. Jazwiec, M. Malinowski, M. R. Bersi, T. A. Timek, M. K. Rausch, A detailed mechanical and microstructural analysis of ovine tricuspid valve leaflets, Acta Biomaterialia 102 (2020-01) 100–113. doi:10.1016/j.actbio.2019.11.039.

[25] K. J. Smith, M. Mathur, W. D. Meador, B. Phillips-Garcia, G. P. Sugerman, A. K. Menta, T. Jazwiec, M. Malinowski, T. A. Timek, M. K. Rausch, Tricuspid chordae tendineae mechanics: Insertion site, leaflet, and size-specific analysis and constitutive modelling, Exp Mech 61 (1) (2021-01) 19–29. doi:10.1007/s11340-020-00594-5.

[26] M. Mathur, W. D. Meador, T. Jazwiec, M. Malinowski, T. A. Timek, M. K. Rausch, Tricuspid valve annuloplasty alters leaflet mechanics, Ann Biomed Eng 48 (12) (2020-12) 2911–2923. doi:10.1007/s10439-020-02586-x.

[27] M. Mathur, W. D. Meador, T. Jazwiec, M. Malinowski, T. A. Timek, M. K. Rausch, The effect of downsizing on the normal tricuspid annulus, Ann Biomed Eng 48 (2) (2020-02) 655–668. doi:10.1007/s10439-019-02387-x.

[28] C. J. Kostelnik, W. D. Meador, C.-Y. Lin, M. Mathur, M. Malinowski, T. Jazwiec, Z. Malinowska, M. L. Piekarska, B. Gaweda, T. A. Timek, M. K. Rausch, Tricuspid valve maladaptation in sheep with biventricular heart failure: The posterior and septal leaflets, pages: 2024.09.16.613284 Section: New Results (2024-09-20). doi:10.1101/2024.09.16.613284.
URL https://www.biorxiv.org/content/10.1101/2024.09.16.613284v1

[29] W. Bothe, E. Kuhl, J.-P. E. Kvitting, M. K. Rausch, S. Göktepe, J. C. Swanson, S. Farahmandnia, N. B. Ingels, D. C. Miller, Rigid, complete annuloplasty rings increase anterior mitral leaflet strains in the normal beating ovine heart, Circulation 124 (11) (2011-09-13) S81–S96. doi:10.1161/CIRCULATIONAHA.110.011163.

[30] E. Ban, P.-D. Kalogerakos, R. Khosravi, B. A. Ziganshin, H. Ellauzi, A. B. Ramachandra, M. A. Zafar, J. D. Humphrey, J. A. Elefteriades, Extended law of laplace for measurement of the cloverleaf anatomy of the aortic root, Int J Cardiovasc Imaging 39 (7) (2023-07-01) 1345–1356. doi:10.1007/s10554-023-02847-5.

[31] A. Gomez, Z. Wang, Y. Xuan, M. D. Hope, D. A. Saloner, J. M. Guccione, L. Ge, E. E. Tseng, Association of diameter and wall stresses of tricuspid aortic valve ascending thoracic aortic aneurysms, J Thorac Cardiovasc Surg 164 (5) (2022-11) 1365–1375. doi:10.1016/j.jtcvs.2021.05.049.

[32] V. Prot, B. Skallerud, Nonlinear solid finite element analysis of mitral valves with heterogeneous leaflet layers, Comput Mech 43 (3) (2009-02) 353–368. doi:10.1007/s00466-008-0310-2.

[33] M. Malinowski, T. Jazwiec, H. Ferguson, J. Bush, M. K. Rausch, T. A. Timek, Tricuspid leaflet kinematics after annular size reduction in ovine functional tricuspid regurgitation, The Journal of Thoracic and Cardiovascular Surgery (2021-02) S0022522321002038doi:10.1016/j.jtcvs.2021.01.104.

[34] A. Basu, C. Lacerda, Z. He, Mechanical properties and composition of the basal leaflet-annulus region of the tricuspid valve, Cardiovasc Eng Tech 9 (2) (2018-06-01) 217–225. doi:10.1007/s13239-018-0343-4.